Surface Potential Model of Double Metal Fin Gate Tunnel FET

Ajay Kumar Dharmireddy[1*], Dr. Sreenivasa Rao Ijjada[2], Dr. I. Hemalatha[3], Dr. Ch. Madhava Rao[4]

[1]Research Scholar, GITAM Institute of Technology, Vishakhapatnam, Andhra Pradesh, 530016, India

[2]Assistant Professor, GITAM Institute of Technology, Vishakhapatnam, Andhra Pradesh,530016, India

[3]Assosiate Professor, SIR C. R. Reddy College of Engineering, Eluru, Andhra Pradesh ,534007,India

[4]Assosiate Professor, SIR C.R.Reddy College of Engineering, Eluru,Andhra Pradesh ,534007,India

[*]Corresponding Author: Ajay kumar Dharmireddy[1]. Email: ajaykumardharmireddy@sircrrengg

Article Info
Page Number: 1044 – 1060
Publication Issue:
Vol. 71 No. 3 (2022)

Article History
Article Received: *12 January 2022*
Revised: *25 February 2022*
Accepted: *20 April 2022*
Publication: *09 June 2022*

Abstract

In this paper, we have proposed a surface model of double material Fin-shape gatetunnel FET (DM Fin TFET) analyzed based on a perimeter-weighted method for low voltage applications. The model obtained by the total device is separated into symmetrical and asymmetrical, and then solved by the 3D Poisson equation. The surface potential and the electrical field are obtained by solving the Poisson equation and the drain current is finally estimated using Kane's model to measure the tunneling generation rate. As compared with exiting model of single metal fin TFET is improved performance of the DM Fin-Gate TFET device i.e., enhanced ON-state current (I_{ON}), and low off-state current (I_{OFF}) and also improved the subthreshold swing(SS) of the proposed device. Our proposed model outputs are evaluated with TCAD device simulation software.

Keywords: Double-metal (DM) gate;FinTFET; Kane's tunneling model; surface potential, electric field,.

1 Introduction

To resolve the constraints of the MOS transistor, TFET has gained significant interest as an alternative device that likely reaches the nanometer dimensions of the MOSFET. The TFET is one of the most successful devices for minimum-consumption power i.e., Because of their least sub-threshold swing (SS) (even the minimum limit for standard MOS transistors is below 60 mV / decade) and low OFF-current. To enrichment of the electrostatic control and adequate ON/OFF performance is one of the most important factors. In these point of view traditional transistor architectures the same as the FinFET[1] are considered to be excellent solutions, because of FinFET has been proven possessing strong gate control ability[2]. These two device combinations are designed to achieve excellent performance. Researchers investigated a sum of possible strategies, for instance low band gap substances[3],metal gate work function, Source(S)/Drain(D) material engineering[4] ,strain channel engineering[5], high-k dielectric (or) partially mixture with SiO2 Gate-oxide engineering[6], and multi-gate techniques[7] to enhance the TFETs drive current.

In this work, an effort has been made to report a 3-D analytical model for the asymmetrical doped channel of SOI based Fin Gate TFETs[8] with a dual gate oxide [9] structure. In this

direction, Kumar et al. suggested a double gate TFET with stacked gate oxide structure to reinforce the ON-current and diminish the SS value while retaining the unchanged OFF-state current value. The gate leakage current [10] could be considerably 6-7 orders reduced by replacement of SiO_2 /HfO_2 gate oxide structure. The need for a dual-material gate (DMG) consists of M_1 (close to source) and M_2 (close drain), with separate work functions, accordingly, ψ_{M1} and ψ_{M2}. For an n-type DMG device, $\psi_{M1}>\psi_{M2}$. In DMG system, the impact of the reduced electrical field in the drain side improves the gate control. The step potential indicates that the drain potential does not affect the potential under M_1. At the same point, the potential under M2 is not controlled by the potential for drain. A high-K dielectric Gate Oxide double Material Fin structure TFET, device parameters along with surface potential and electrical fields addressed in this model. The Drain current is assessed using Kane band-to-band tunneling model [11] in TFET's. Finally, the effect of the different gate oxide thicknesses and the channel carrier doping concentrations [12] on the drain current also evaluated.

2. Working Mechanism of TFET:

The vital structure of tunnel FET has a p-i-n junction channel architecture. Figure1. Shows the standard TFET device extremely doped with p+ region of the source, the intermediate doped of the n-type channel and also the highly doped n-type drain. Generally, TFET present includes different parameters like I_{GEN}, I_{BTBT} and I_s. I_{GEN} is generation current which is dependent upon the creation of holes and electrons at the depletion areas, is a part of reverse-biased voltage. I_{BTBT} is also band-to-band tunneling current which is dependent upon the tunneling of this carrier in the occupied band of this origin to an empty group of the station. I_s really is a reverse saturation current which is based on the diffusion part of the current.

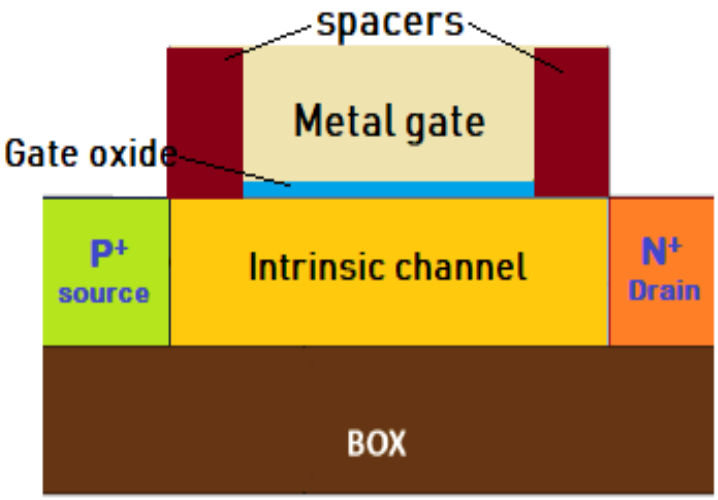

Figure 1.Schematic diagram of Tunnel FET structure.

I-V characteristics of TFET has two states one is OFF-state and another one ON state is shown in Figure 2.In this off-sate gate is fully depleted the channel and also tunnel barrier length is very large because of small applied gate bias voltage. The leakage (Ioff) current of the TFETs has very low (lower than the usual couple of pA/ µm). In this ON state when the gate bias voltage exceed the threshold voltage gradually decrease barrier length and also flow

the conduction current (Ion) in between conduction and valance band of device.The gate bias exceeds beyond the limit in between band gap a path in the valence to conduction band will emerge near the source. The tunnel distance much reduced as compared to the amount of the intrinsic region and also an affected in BTBT and raises the conduction (I_{ON}) current of drain-source.

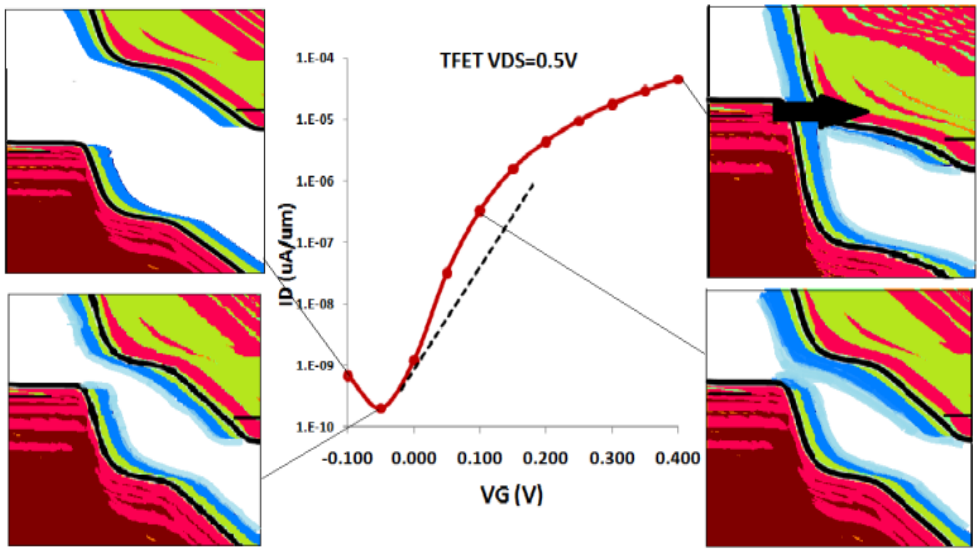

Figure 2. I-V characteristics with the different gate bias

2.1 Literaturesurvey

Kaishen Ou et al.[13] demonstrated structure for p-type Ge-Fin TFET with a wrapped around epitaxial layer is shown in Figure 3.The limitations are too large gate-source overlap can compromise drive current due to increased series resistance in the larger undoped epitaxial layer beneath the gate. Low temp. (330 ~ 400 ˚C) growth of Ge is preferred.

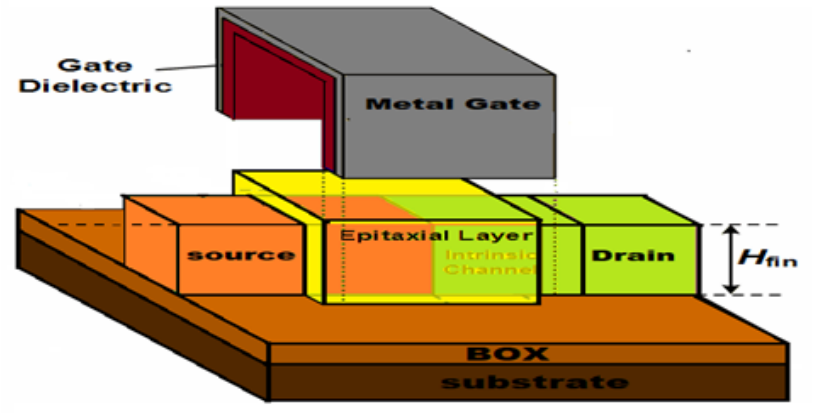

Figure 3. SiGe based FinTFET.

The influence of the height (H_{fin}) and width (W_{fin}) of a Si fin on the Epitaxial layer TFETs [13]. Because the EL is formed on the top and sidewall of a fin, the vertical BTBT cross-sectional area is proportional to H_{fin}. Therefore, the increase of Hf_{in} leads to Ion boosting in the case of EL TFETs.

Priyanka Saha et al., [14] explained that Dual Metallic TG TFET will be It's been proven to research tunneling distance tuning from the station area by double gate dielectric with different values of work functions of metal 1&2 that BTB carrier tunneling at the origin into the station region enriches the BTB provider tunneling out of the origin to the station area with significant advancement in Ion/Ioff that the ratio will be 10^2, the low threshold voltage.

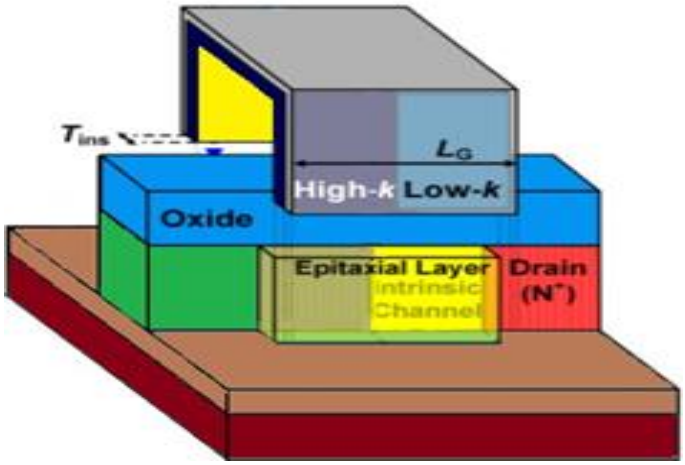

Figure 4. GHG TFET [15].

Jang Hyun Kim et al. [16] suggested TFET comes with a SiGe channel, a fin arrangement along with a raised drain to boost its electrical operation. It reveals I_{ON} is improved by twenty four times of silicon and six times more of silicon-germanium. The ambipolar current (I_{AMB}) can be decreased by 900 times compared with SiGe.

K.-H. Kao et al. [17] , the fully overlapped device manufacture the high ON- currents, however. ON-current distinctions for the three types of TFET line tunneling. It in the main depends on supply concentration and Equivalent compound thickness (EOT) factors to decrease tunnel path.

3. Device Structure

A 3-D view of the DM Fin TFET structure is shown in Figure 6.The asymmetric intrinsic channel is highly doped with source side and lightly doped with drain side [18]. Two different gates M1 and M2 are utilized in the DM Fin-gate TFET [19], with the lengths L1 and L2, correspondingly, and the total length of the gate is L = L1+L2. A higher work function (ψM1) of L1 is close to the source-end and lower work function (ψ_{M1}) of L2 is adjacent to the drain-end performance as control and screening gate. The fin thickness is T_{si} and fin height is H_{fin} respectively.

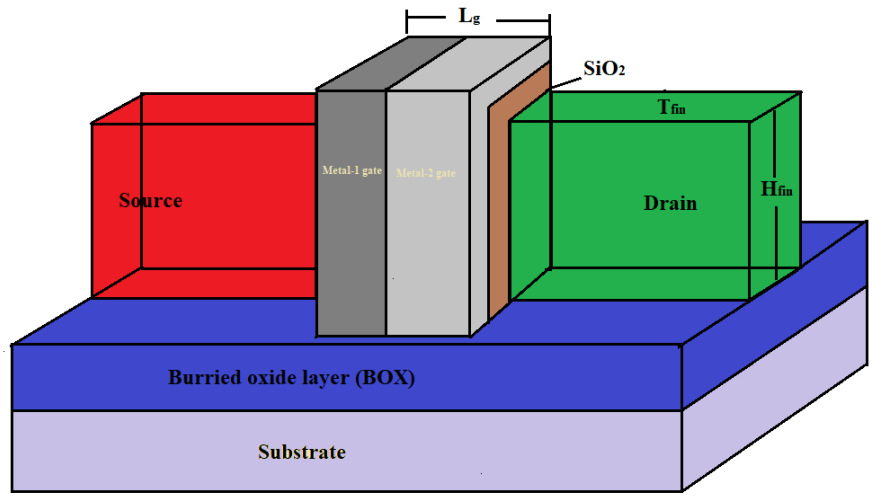

Figure 5. 3D view of the Double Metal Fin gate Tunnel FET

4. MODEL FORMATION

4.1 Surface Potential Model

The potential distribution inside the channel is attained by resolving 3D Poisson equation [20] with suitable constraints at the gate oxide interfaces and near source / drain ends. The total 3D structure separated into an asymmetric 2D device and symmetric 2D device .A 3D potential distribution is derived from perimeter-weighted sum method [21].

The 3D Poisson's condition along weak inversion region of channel can be express as:

$$\frac{\partial^2\psi(x,y,z)}{\partial x^2}+\frac{\partial^2\psi(x,y,z)}{\partial y^2}+\frac{\partial^2\psi(x,y,z)}{\partial z^2}=\frac{qN_A}{\varepsilon_{si}};\ 0\le x\le T_{si};\ 0\le y\le H_{fin};\ \text{and}\ 0\le z\le L, \quad (1)$$

Concept on initial conditions:

$$\psi_1(x,y,0)=V_{bi,p} \quad (2)$$

$$\psi_2(x,y,L_1+L_2)=V_{bi,n}+V_{ds} \quad (3)$$

Where $V_{bi,p}=-V_t\ln\left(\frac{N_a}{N_{ch}}\right)$; $V_{bi,n}=V_t\ln\left(\frac{N_dN_{ch}}{n_i^2}\right)$

Here the total length (L)=L_1+$L_2$and N_a, N_d are doping concentration of source side and drain side, 'V_t'is the thermal voltage and 'n_i' is the concentration of intrinsic carrier.

$$\left.\frac{d\psi_1(x,y,z)}{dy}\right|_{y=0}=\left(\frac{\varepsilon_{ox}}{\varepsilon_{si}}\right)\left(\frac{\psi_{s1}(x,0,z)-V'_{GS1}}{t_{ox}}\right); \quad (4)$$

$$\left.\frac{d\psi_2(x,y,z)}{dy}\right|_{y=0}=\left(\frac{\varepsilon_{ox}}{\varepsilon_{si}}\right)\left(\frac{\psi_{s2}(x,0,z)-V'_{GS2}}{t_{ox}}\right); \quad (5)$$

$$\left.\frac{d\psi_1(x,y,z)}{dy}\right|_{y=H_{fin}}=\left(\frac{\varepsilon_{ox}}{\varepsilon_{si}}\right)\left(\frac{V'_{SUB}-\psi_B(x,H_{fin},z)}{t_{oxb}}\right); \quad (6)$$

$$\left.\frac{d\psi_2(x,y,z)}{dy}\right|_{y=H_{fin}}=\left(\frac{\varepsilon_{ox}}{\varepsilon_{si}}\right)\left(\frac{V'_{SUB}-\psi_B(x,H_{fin},z)}{t_{oxb}}\right); \quad (7)$$

$$\left.\frac{d\psi_1(x,y,z)}{dy}\right|_{x=0}=\left(\frac{\varepsilon_{ox}}{\varepsilon_{si}}\right)\left(\frac{\psi_{s1}(0,y,z)-V'_{GS1}}{t_{ox}}\right); \quad (8)$$

$$\left.\frac{d\psi_2(x,y,z)}{dy}\right|_{x=0}=\left(\frac{\varepsilon_{ox}}{\varepsilon_{si}}\right)\left(\frac{\psi_{s2}(0,y,z)-V'_{GS2}}{t_{ox}}\right); \quad (9)$$

$$\left.\frac{d\psi_1(x,y,z)}{dy}\right|_{x=T_{si}}=\left(\frac{\varepsilon_{ox}}{\varepsilon_{si}}\right)\left(\frac{V'_{GS1}-\psi_{s1}(T_{si},y,z)}{t_{ox}}\right); \quad (10)$$

$$\left.\frac{d\psi_2(x,y,z)}{dy}\right|_{x=T_{si}} = \left(\frac{\varepsilon_{ox}}{\varepsilon_{si}}\right)\left(\frac{V'_{GS2}-\psi_{s2}(T_{si},y,z)}{t_{ox}}\right); \quad (11)$$

The potential distribution and electric fields in between two metals are continuous

$$\psi_1(x,y,L_1) = \psi_2(x,y,L_1); \quad (12)$$

$$\left.\frac{d\psi_1(x,y,z)}{dy}\right|_{z=L_1} = \left.\frac{d\psi_2(x,y,z)}{dy}\right|_{z=L_1}; \quad (13)$$

Where ψ is the total channel potential of $\psi_1$and ψ_2 are the channel potential of M_1 and M_2.$\psi_{S1}$and ψ_{S2} are the potential distribution of M_1&M_2 respectively. ψ_b is the backend oxide conjunction with silicon interface potential, V_{ds} is the drain to source voltage and V_{bi} is the built in potential.

$V'_{gs} = V_{gs} - V_{fb,f}$ and $V'_{sub} = V_{sub} - V_{fb,b}$,

Where V_{gs} ,V_{sub} are the gate-source and substrate voltage, $V_{fb1,f}$ and $V_{fb2,f}$ are the front end channel flat-band potential for M_1 and M_2, correspondingly, and $V_{fb,b}$ is the flatband potential of back end channel. Dual metal gate flat-band voltagesV_{fb1}(or)ψ_{MS1}andV_{fb2} (or) $\psi_{MS2}$are specified as difference between potential of M_1 (or) M_2 and surface work function (ψ_s) .

$$\text{work function of the semiconductor } (\psi s) = \aleph_{si} + \frac{E_g}{2q} + \psi_F \quad (14)$$

$$\text{Fermi potential } (\psi_F) = \psi_t \ln\left(\frac{N_a}{n_i}\right)$$

Where ψ_t is the thermal potential and $\aleph_{si}$ is the electron affinity.

4.2 Potential for the asymmetric DM TFET

The asymmetric DM TFET potential distribution within the weak inversion region are often calculated by resolving the 2D Poisson equation [22], it's possible to write as

$$\frac{\partial^2\psi(y,z)}{\partial y^2} + \frac{\partial^2\psi(y,z)}{\partial z^2} = \frac{qN_a}{\epsilon_{si}}. \qquad 0 \le Y \le H_{fin},\ 0 \le Z \le L \quad (15)$$

With boundary conditions

$$\left.\frac{d\psi_1(y,z)}{dy}\right|_{y=0} = \left(\frac{\varepsilon_{ox}}{\varepsilon_{si}}\right)\left(\frac{\psi_{s1}(z)-V'_{gs1}}{t_{ox}}\right); \quad (16)$$

$$\left.\frac{d\psi_2(y,z)}{dy}\right|_{y=0} = \left(\frac{\varepsilon_{ox}}{\varepsilon_{si}}\right)\left(\frac{\psi_{s2}(z)-V'_{gs2}}{t_{ox}}\right); \quad (17)$$

$$\left.\frac{d\psi_1(y,z)}{dy}\right|_{y=H_{fin}} = \left(\frac{\varepsilon_{ox}}{\varepsilon_{si}}\right)\left(\frac{V'_{sub}-\psi_b(z)}{t_{oxb}}\right); \quad (18)$$

$$\left.\frac{d\psi_2(y,z)}{dy}\right|_{y=H_{fin}} = \left(\frac{\varepsilon_{ox}}{\varepsilon_{si}}\right)\left(\frac{V'_{sub}-\psi_b(z)}{t_{oxb}}\right); \quad (19)$$

$$\psi_1(0, L_1) = \psi_2(0, L_1) \quad (20)$$

$$\left.\frac{d\psi_1(y,z)}{dz}\right|_{z=L1} = \left.\frac{d\psi_2(y,z)}{dz}\right|_{z=L1} \quad (21)$$

$$\psi_1(0, 0) = \psi_{S1}(0) = V_{bi,p} \quad (22)$$

$$\psi_2(0, L_1 + L_2) = \psi_{S2}(L_1 + L_2) = V_{bi,n} + V_{ds} \quad (23)$$

The potential distribution function in the perpendicular 'y' direction presumed as parabolic by giving the Young method[23]:

$$\psi_i(y, z) = \psi_{Si}(z) + p_{i1}(z)\, y + p_{i2}(z)\, y^2, \quad (24)$$

Where i= 1,2 and $p_{i1}(z)$and $p_{i2}(z)$are coefficients of z only.

For the DMmodel, the potential distribution of M_1 and $M_2$are given by:

$$\psi_1(y, z) = \psi_{s1}(z) + p_{11}(z)\, y + p_{12}(z)\, y^2;\ 0 \le y \le H_{fin},\ 0 \le z \le L_1 \quad (25)$$

$\psi_2(y, z) = \psi_{s2}(z) + p_{21}(z)\, y + p_{22}(z)\, y^2$; $0 \le y \le H_{fin}$, $L_1 \le z \le L_1 + L_2$ (26)

Put on the boundary conditions (16) to (19), we get the coefficients:

$$P_{11}(z) = \frac{Cox}{\epsilon_{si}}(\psi_{s1}(z) - V'_{gs1}); \quad (27)$$

$$P_{21}(z) = \frac{Cox}{\epsilon_{si}}(\psi_{s2}(z) - V'_{gs2}); \quad (28)$$

$$P_{12}(z) = \frac{\left[V'_{sub} - \left(1 + \frac{C_{ox}}{C_{oxb}} + \frac{C_{ox}}{C_{si}}\right)\psi_{S1}(z) + \left(\frac{C_{ox}}{C_{oxb}} + \frac{C_{ox}}{C_{si}}\right)V'_{gs1}\right]}{\left[1 + \frac{2C_{si}}{C_{oxb}}\right]H_{fin.}}; \quad (29)$$

$$P_{22}(z) = \frac{\left[V'_{SUB} - \left(1 + \frac{C_{ox}}{C_{oxb}} + \frac{C_{ox}}{C_{si}}\right)\psi_{S2}(z) + \left(\frac{C_{ox}}{C_{oxb}} + \frac{C_{ox}}{C_{si}}\right)V'_{GS2}\right]}{\left[1 + \frac{2C_{si}}{C_{oxb}}\right]H_{fin}^2}; \quad (30)$$

Where $C_{ox} = \frac{\varepsilon_{HfO2}}{t_{eff}}$; $C_{si} = \frac{\varepsilon_{si}}{H_{fin}}$; $C_{oxb} = \frac{\varepsilon_{ox}}{t_{oxb}}$; $t_{eff} = t_{sio2} + \frac{\varepsilon_{siO2}}{\varepsilon_{HfO2}} t_{HfO2}$;

Here, the effective oxide thickness (t_{eff}) [24] considered in silicon dioxide thickness (t_{SiO2}) and hafnium dioxide thickness (t_{HfO2}), permittivity of low dielectric (ε_{SiO2}), permittivity of high dielectric (ε_{HfO2}) and permittivity of silicon(ε_{si}).

Substituting all these coefficients in (15), we get:

$$\frac{d^2\psi_{s1}(z)}{dz^2} - \alpha\psi_{s1}(z) = \beta_1; \quad (31.a)$$

$$\frac{d^2\psi_{s2}(z)}{dz^2} - \alpha\psi_{s2}(z) = \beta_2; \quad (31.b)$$

Applying (31), we get$\psi_{S1}(z)$ and $\psi_{S2}(z)$ are:

$\psi_{S1}(z) = A \exp(\lambda_1 z) + B \exp(\lambda_2 z) - \beta_1/\alpha$; (32.a)

$\psi_{S2}(z) = C \exp(\lambda_1(z - L_1)) + D \exp(\lambda_2(z - L_1)) - \beta_2/\alpha$, (32.b)

From 31(a) and 31(b) the values of α, β_1, β_2 and constants are given in the Appendix A.

In order to attain an ample explanation of adequate the boundary conditions in the middle of the source and drain channel inside the silicon fin at changed distance y from the front-gate. We predictable a relationship between $\psi_{S1}(z)$ and $\psi_y(z)$ within M1 at a height y equivalent to portion n of the H_{fin} [24]. A relationship is obtained by replacing the Y is equal to Hfin / n where $n \neq 0$) in (25) between $\psi_{S1}(z)$ and $\psi y(z)$.

Now, replacing $n = y/H_{fin}$, thepotential distributionof the asymmetric DM TFET[25] is attained within M1 as:

$\psi_{asym1}(y, z) = A_1 \exp(\lambda_{1a} z) + B_1 \exp(\lambda_{2a} z) + \sigma_{asym1}$ (33)

In the same way, the potential distribution of asymmetric DM TFET within M_2 as:

$\psi_{asym2}(y, z) = C_1 \exp(\lambda_{1a}(z - L_1)) + D_1 \exp(\lambda_{2a}(z - L_1)) + \sigma_{asym2}$, (34)

where $\sigma_{asym1} = -\beta_{asym1}/\alpha_{asym}$, $\sigma_{asym2} = -\beta_{asym2}/\alpha_{asym}$,$\lambda_{1a} = \sqrt{\alpha_{asym}}$; $\lambda_{2a} = -\sqrt{\alpha_{asym}}$

the values of α_{asym} , β_{asym1} , β_{asym2}, A_1, B_1,$C_1$and $D_1$are given Appendix B.

Due to the existence of greater work function in M_1,asymmetric DM TFET minimum potential shall exist i.e., $\psi_{asym,min} = 2\sqrt{A_1 B_1} + \sigma_{asym1}$ (35)

The electric field for asymmetric DM TFET under M1 is computed in z direction as

$E_{asym1}(y, z) = A_1\lambda_{1a} \exp(\lambda_{1a}(z)) + B_1\lambda_{2a} \exp(\lambda_{2a}(z))$ (36)

Similarly, The electric field for asymmetric DM TFET under M2 in the direction of z is calculated from $d\psi_{asym2}/dz \mid y = 0$, by the following:

$E_{asym2}(y, z) = C_1\lambda_{1a} \exp(\lambda_{1a}(z - L_1)) + D_1\lambda_{2a} \exp(\lambda_{2a}(z - L_1))$ (37)

4.3 Potential for symmetric DM TFET

The potential for a symmetric DM TFET (ψ(x, z)) will be calculated in the same way as asymmetric case, Substitute y for x,H_{fin}forT_{si}, t_{oxb}fort_{ox}, and V_{sub}forV_{gs}.

A symmetric case for potential distribution under M_1 and M_2 are specified as:

$$\psi_{sym1}(x, z) = A_2\exp(\lambda_{1s}z) + B_2\exp(\lambda_{2s}z) + \sigma_{sym1} \quad (38)$$

$$\psi_{sym2}(x, z) = C_2\exp(\lambda_{1s}(z - L_1)) + D_2\exp(\lambda_{2s}(z - L_1)) + \sigma_{sym2}, \quad (39)$$

At this point $\sigma_{sym1} = -\frac{\beta_{sym1}}{\alpha_{sym}}$, $\sigma_{sym2} = -\frac{\beta_{sym2}}{\alpha_{sym}}$and $\lambda_{1s} = \lambda_{2s} = \sqrt{\alpha_{sym}}$.

The limitsof asymmetric caseα_{asym}, β_{asym1}, and $\beta_{asym2}$are attained fromsymmetric case of α_{sym}, β_{sym1}, and β_{sym2}, respectively, by substituting $C_{si}$for$C_T$and $C_{oxb}$for C_{ox}, including the above mention derivation.

Also, the constants A_2, B_2, C_2, and D_2 are attained from A_1, B_1, C_1, and D_1, respectively, by replacing λ_{1asym}forλ_{1sym}, λ_{2asym}forλ_{2sym}, $\sigma_{asym1}$for σ_{sym1}, and σ_{asym2}forσ_{sym2}.

Smearing the condition $d\psi_{sym1}/dz\,|_{z=0}$ in (38), we attain the minimum potential of symmetric case is:$\psi_{sym,min} = 2\sqrt{A_2B_2} + \sigma_{sym1}$ (40)

The derivative of symmetric case potential distribution function w.r.to z at limit z=0 , get the DM TFET electric field component at drain end is

$$E_{sym2}(x, z) = C_2\lambda_{1s}\exp(\lambda_{1s}(z - L_1)) + D_2\lambda_{2s}\exp(\lambda_{2s}(z - L_1)) \quad (41)$$

4.4 Potential for the DM Fin-gate TFET

In the DM Fin-gate TFET, the potential distribution is represented as the perimeter-weighted sum of $\psi_{asym1}(y, z)$ and $\psi_{sym1}(x, z)$ underneath of M_1, and ($\psi_{asym2}(y, z)$ and $\psi_{sym2}(x, z)$) underneath of M_2, as shown below:

$$\psi_1(x, y, z) = \left(\frac{T_{Si}}{T_{si}+2H_{fin}}\right)\psi_{asym1}(y, z) + \left(\frac{2H_{fin}}{T_{si}+2H_{fin}}\right)\psi_{sym1}(x, z) \quad (42)$$

$$\psi_2(x, y, z) = \left(\frac{T_{Si}}{T_{si}+2H_{fin}}\right)\psi_{asym2}(y, z) + \left(\frac{2H_{fin}}{T_{si}+2H_{fin}}\right)\psi_{sym2}(x, z) \quad (43)$$

$$\psi_{S,min} = \left(\frac{T_{Si}}{T_{si}+2H_{fin}}\right)\psi_{asym,min} + \left(\frac{2H_{fin}}{T_{si}+2H_{fin}}\right)\psi_{sym,min} \quad (44)$$

$$E_F(x, y, z) = \left(\frac{T_{Si}}{T_{si}+2H_{fin}}\right)E_{asym2}(y, z) + \left(\frac{2H_{fin}}{T_{si}+2H_{fin}}\right)E_{sym2}(x, z), \quad (45)$$

Where $\psi_{S,min}$is the minimum potential distribution and $E_F(x, y, z)$ is electric field at the drain side.

Based on kane's method calculate tunnelling current (I_D)[21] which is done by assimilating the BTB generation rate of carriers (G_{BTB})[22] on the device volume.

In this model we using BTB approach.

$$I_{BTBT} = q\int G_{BTB}dV = q\int \mathcal{A}\frac{|E_F|^{\mathcal{G}}}{E_g^{1/2}}\exp\left(-\mathcal{B}\frac{E_g^{3/2}}{|E_F|}\right)dV. \quad (46)$$

Where $\mathcal{A} = \frac{q^2\sqrt{2m_{tunel}}}{h^2\sqrt{E_g}}$; $\mathcal{B} = \frac{\pi^2E_g^{3/2}\sqrt{m_{tunnel}/2}}{qh}$; $m_{tunnel} = \frac{m_0m_em_h}{m_e+m_h}$;

Where , $\boldsymbol{\mathcal{A}}$ and $\mathcal{B}$ are are defined by material dependent Kane parameters, band gap materials and effective electron (or) hole mass. Regional and average electrical fields (Eavg)[23] are indicated in the E_F component. Here m0 is the portion of the mass electron and m_e,m_h are the effective mass of electrons and holes.

The current submitted to the Source- tunneling junction underneath M_1 can be described as

$$I_{s-c} = \int_0^{t_{si}} \int_0^{H_{fin}} \int_{Z_{s1}}^{Z_{s2}} \mathcal{A}\, E_s E_{avg}^{\mathcal{G}_1 - 1} \exp\left(\frac{-\mathcal{B}}{E_{avg}}\right) dxdydz \quad (47)$$

Here Electric field in average $(E_{avg}) = \frac{E_g}{q.I_{s,path}}$ and $E_S = \sqrt{E_{x_1}^2 + E_{y_1}^2 + E_{z_1}^2}$ is the total electric field in region 1 below M_1 at thesource channel junction .

$I_{s,tunnel} = Z_{s2} - Z_{s1}$. Present the successful tunneling length atjunction of source-channel with Z_{S1} is the distance between tunneling start from source valance band (VB) to channel conduction band (CB) and Z_{S2} is the channel location where tunneling ends.

Where $Z_{s1} = \frac{E_g + E_{VS} - E_{FS} - A_1 - B_1 - (H_1/G)}{q\sqrt{G}(A_1 - B_1)}$;

(48)

Here E_{VS} and E_{FS} are source VB and Fermi level of source side.Similarly, the total electric field of fin gate TFET $(E_D) = \sqrt{E_{x_2}^2 + E_{y_2}^2 + E_{z_2}^2}$ at region-2 the tunneling at drain-channel junction (i.e., $I_{D,tunnel} = Z_{d2} - Z_{d1}$)is also accountable.

Where $Z_{d2} = \frac{E_g + E_{VS} - E_{VC} - A_2 - B_2 - (H_2/G)}{\sqrt{G}(A_2 - B_2)}$;

(49)

The current contributions due to carriers tunneling at thejunction of Drain-channel underneath M_2 can be described as

$$I_{D-c} = q \int_0^{t_{si}} \int_0^{H_{fin}} \int_{Z_{d1}}^{Z_{d2}} \mathcal{A}\, E_d E_{avg}^{\mathcal{G}_2 - 1} \exp\left(\frac{-\mathcal{B}}{E_{avg}}\right) dxdydz \quad (50)$$

From now, total tunneling current $(I_{tunnel}) = I_{tunnel,S-c} + I_{tunnel,D-c}$ (51)

The tunneling current (I_{tunnel}) from equ.(57) and input voltage (V_{gs}) can be evaluate an Subthreshold swing of device is defined as:

Subthreshold swing(S) $= \frac{\partial V_{GS}}{\partial \log I_D} = \left[\frac{\partial \log I_{tunnel}}{\partial V_{GS}}\right]^{-1}$

(52)

The high speed devices require low SS value. That is the characteristics of the device must be steeper for fast switching of the device. Fast switching from ON to OFF more suitable for low power applications

5.RESULTS DISCUSSION

In this section, based on analytical model derived and the simulated results, we reported the channel potential, electrical field and drain current of proposed device. BTBT current is developed by using the Kane model. To validate the accuracy of our derived model, TCAD simulator [29] data were given. For the simulation of the proposed device SRH recombination model [30] and dynamic barrier tunneling model [31] were supported. We used the device parameters as set out in Table 1. Figure 2 is shown 3D simulated output of the proposed device.

Table 1 Device simulation parameters

Parameter	**Values**
Doping Concentration of drain side (N_d)	10^{18} cm−3
Doping Concentration of source side (N_s)	10^{20} cm−3
Doping Concentration of Channel (N_{ch})	10^{17} cm−3

Length of the Channel (L)		40nm
Gate metal-1 (Cobalt) work function	4.7ev	
Gate metal-2 (Aluminium) work function		4.1ev
Gate oxide (SiO_2) thickness	3nm	
BOX thickness (t_{box})	50nm	
Fin width W_{fin} (T_{si})		40nm
Fin height (H_{fin})	20nm	
Metal-1&2 length		20nm

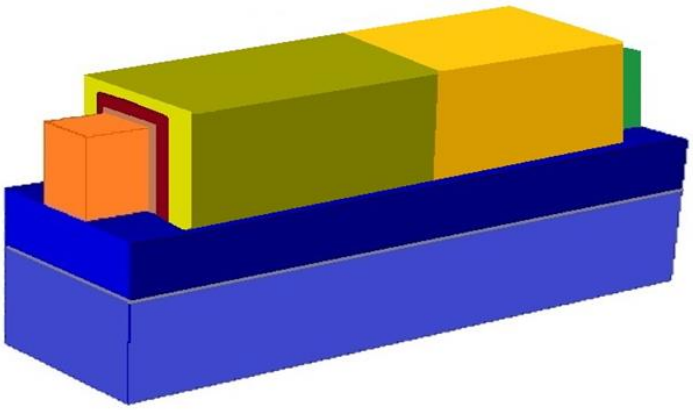

Figure 6. Simulated 3D structure of Dual gate oxide DM Fin TFET structure

5.1 Transfer characteristics

The Id – Vgs characteristics of double metal Fin TFET with work function of metal-1 (Ψ_{M1}) is 4.7 eV, metal-2 (Ψ_{M2}) is 4.1 eV as associated with single metal(SM) gate Fin TFET with double gate oxide is shown in Figure 7. The difference in the drain current with respect to various input bias (V_{gS}) at V_{dS}=0.05 V. There is a significant progress in on-state current is 10^{-4} A/m and off state current 10-14 A/m in DM Fin TFET and 10^{-6} A/m and off state current 10^{-15} A/m in SM Fin TFET. Therefore, the DMG FinTFET provides improved SS as compared to a conventional SMG FinTFET.

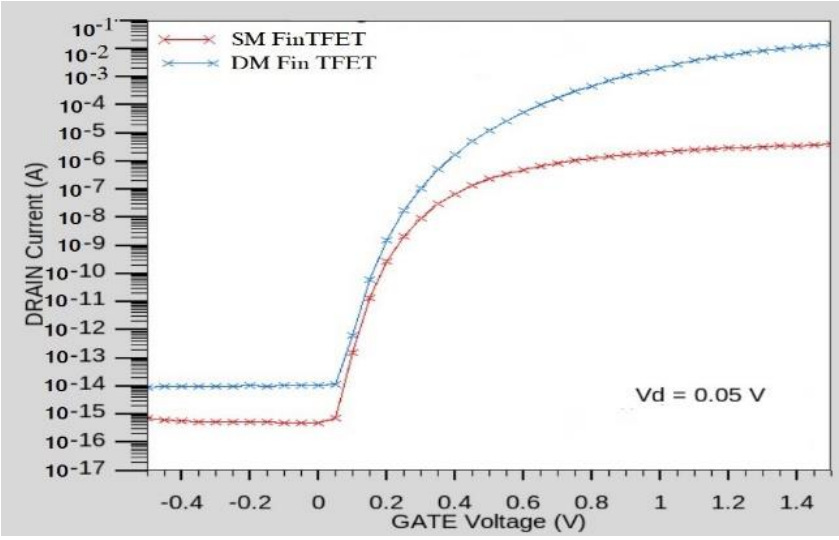

Figure 7. I_d – V_{GS} characteristics of SM Fin TFET and DM Fin TFET.

5.2 Surface potential

In this proposed TFET device dual metal gate arrangement is source side connected to the low work function (Ψ_{M1}) gate material and drain side connected to the high work function (Ψ_{M2}) gate material. Gradual improvement of potential which is tunneling mechanism of drive current at the source and channel junction by use source side lower work function of gate metal. Figure 8. Shows the surface potential of DM Fin TFET compare with SM Fin TFET of Ψ_{M1} (or) Ψ_{M2} is 4.1 eV (or) 4.7eV structures with varying input bias and fixed at drain bias of 0.5 V. However, the use of dual material principle also tends to optimize the OFF state leakage present in the Fin Gate structure.

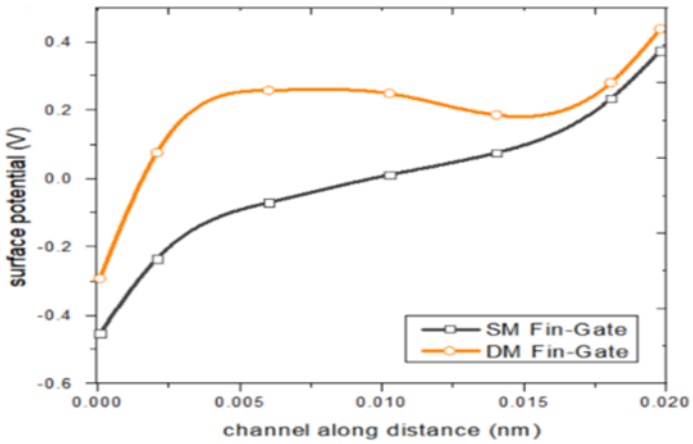

Figure 8. Surface potential distribution along with channel distance at different V_{gs} and V_{ds}=0.5V of SMG and DMG work function (Ψ_{M1} and Ψ_{M2}).

5.3 Total Electric Field

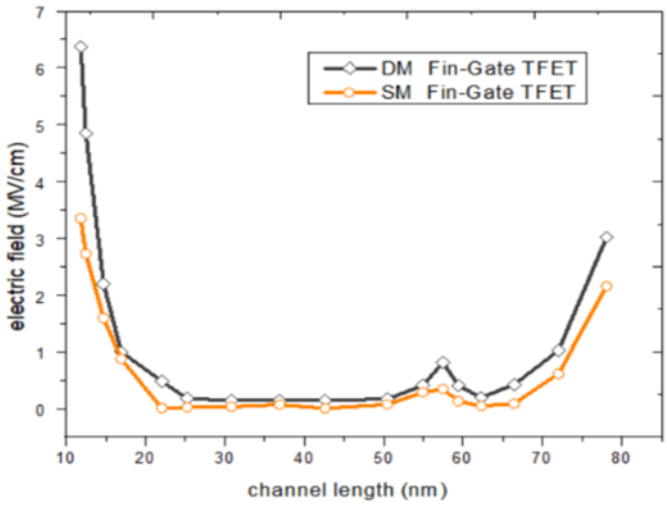

Figure 9. Electric field along the channel distance in SM and DM Fin TFET structures. at V_{gs}=V_{ds}=0.5V.

The higher tunneling probability takes place in source – channel junction by use of dual dielectric materials that result higher electric field occurred in source end and also improving device conduction current. Due to the lower electric field, significantly reduce the ambipolar current at the drain end.

Figure 9. represents a contrast of total electric field with regards to channel location for a single metal gate work function of M1 (Ψ_{M1}) has low electric field as compared with double metal gate Ψ_{M1} and Ψ_{M2} of Fin-gate TFET. As compare with source side gate work function is higher than drain side at $V_{gs}=V_{ds}=0.5V$.The tunneling probability of source side junction increase that effected on improving total electric field of DM FinTFET. The device's ambipolar current reduced by negative electric field at drain end which leads to delay the carriers.

Table 2. Comparison of Proposed model with existing models

TFET Structure [Reference]	Device Parameters (units)			
SS $\left(\frac{\mathbf{mV}}{\mathbf{dec}}\right)$	$\mathbf{I_{ON}}\left(\frac{\mu\mathbf{A}}{\mu\mathbf{m}}\right)$	$\mathbf{I_{OFF}}\left(\frac{\mu\mathbf{A}}{\mu\mathbf{m}}\right)$	$\frac{\mathbf{I_{ON}}}{\mathbf{I_{OFF}}}$	
SG TFET Ref.[1]	74	12.1	10^{-4}	10^{5}
Ref.[2]	61.5	10^{3}	10^{-11}	10^{8}
DG TFET Ref.[12]	52	14.8	10^{-10}	10^{9}
Ref.[3]	41.2	10^{-8}	10^{-17}	10^{11}
SM Fin TFET Ref.[6]	25	10^{-6}	10^{-14}	10^{8}
DM Fin TFET (Proposed model)	21	10^{-4}	10^{-15}	10^{11}

5. Conclusion

This paper proposes analytical modeling of Double Metal Fin gate TFET structure. Surface potential, total electric field and I_{tunnel} are developed on the basis of 3D Poisson equation. As compare with single metal fin gate architecture device has conduction current 10^{-6} μA/μm, leakage current 10^{-14} A/m and SS value 25 mv/decade, Double gate engineering results in an improved the performance of proposed device in terms of subthreshold slope is 21mv/decade, ON-current is 10^{-4} μA/μm and OFF current 10^{-15} A/m is shown in the table 2. The empirical outcomes are in near contract with simulated data from TCAD sentaurus thus confirming our model accuracy.

Conflicts of Interest:

The authors declare that they have no conflicts of interest to report regarding the present study or personal relationships that could have appeared to influence the work reported in this paper.

ORCID iD

ajaykumar dharmireddy:https://orcid.org/0000-0002-5074-4775

References

1. Ritzenthaler, R. et al. (2011) '3D analytical modelling of subthreshold characteristics in vertical Multiple-gate FinFET transistors', Solid-State Electronics. Elsevier Ltd, 65–66(1), pp. 94–102. doi: 10.1016/j.sse.2011.06.023.
2. Dharmireddy, A., Ijjada, R. and Tejomurthy, P. H. S. (2019) 'Performance analysis of Tri-Gate SOI FINFET Structure with various fin heights using TCAD Simulation',Journal of Advanced Research in Dynamical and Control Systems, 11(2), pp. 1291–1297.
3. Yeh, Wen-Kuan (2018). "The Impact of Fin Number on Device Performance and Reliability for Multi-Fin Tri-Gate n- and p-Type FinFET". Transactions on Device and Materials Reliability 18(4), pp. 555–560.
4. Wang, H. et al. (2019) 'Improved Performance in GeSn/SiGeSn TFET by Hetero-Line Architecture With Staggered Tunneling Junction', IEEE Transactions on Electron Devices. IEEE, 66(4), pp. 1985–1989. doi: 10.1109/TED.2019.2898328.
5. Vimala, P and T S Samuel (2020). 'TCAD Simulation Study of Single-, Double-, and Triple-Material Gate Engineered Trigate FinFETs' Semiconductors, 54(4), pp. 501–505.
6. Gaynor, B. D. and Hassoun, S. (2014) 'Fin shape impact on FinFET leakage with application to multithreshold and ultralow-leakage FinFET design', IEEE Transactions on Electron Devices, 61(8), pp. 2738–2744. doi: 10.1109/TED.2014.2331190.
7. Anjali devi N., Dharmireddy, A. and Ijjada, S. R. (2019) 'Performance Analysis of Double Gate Hetero Junction Tunnel Fet', (2), pp. 232–234. doi: 10.35940/ijitee.B1058.1292S319.
8. Vanitha, D. D. . (2022). Comparative Analysis of Power switches MOFET and IGBT Used in Power Applications. International Journal on Recent Technologies in Mechanical and Electrical Engineering, 9(5), 01–09. https://doi.org/10.17762/ijrmee.v9i5.368
9. Ajay kumar Dharmireddy,Sreenivasa rao ijjada (2021) 'A Novel design of SOI based Fin Gate TFET", 2021 2nd Global Conference for Advancement in Technology (GCAT),IEEE pp. 1–4. doi: 10.1109/GCAT52182.2021.9587599.
10. Bose, Ria (2020), Analytical model and simulation-based analysis of a work function engineered triple metal tunnel field-effect transistor device showing excellent device performance' IET Circuits, Devices & Systems published by John Wiley & Sons Ltd.; pp.1–9.
11. Saha, R., Bhowmick, B. and Baishya, S. (2019) 'Analytical threshold voltage and subthreshold swing model for TMG FinFET', International Journal of Electronics. Taylor & Francis, 106(4), pp. 553–566. doi: 10.1080/00207217.2018.1545258.
12. Nigam, K. et al. (2018) 'Controlling the ambipolarity and improvement of RF performance using Gaussian Drain Doped TFET', International Journal of Electronics. Taylor & Francis, 105(5), pp. 806–816. doi: 10.1080/00207217.2017.1409807.
13. Devi N.A,Ajay K D, A. and Member, S. (2020) 'Performance Characteristics of Tfet over Mosfet , Dg- Mosfet and Finfet',TEST engineering & Managament Magine82(1), pp. 6164–6170.
14. Malla, S., M. J. . Meena, O. . Reddy. R, V. . Mahalakshmi, and A. . Balobaid. "A Study on Fish Classification Techniques Using Convolutional Neural Networks on Highly Challenged Underwater Images". International Journal on Recent and Innovation Trends in Computing and Communication, vol. 10, no. 4, Apr. 2022, pp. 01-09, doi:10.17762/ijritcc.v10i4.5524.
15. Komalavalli, S., Arun Samuel, T. S. and Vimala, P. (2019) 'Performance analysis of triple material tri gate TFET using 3D analytical modelling and TCAD simulation', AEU -

International Journal of Electronics and Communications. Elsevier GmbH, 110, p. 152842. doi: 10.1016/j.aeue.2019.152842.

16. Ou, Kaishen and Chunxiang Zhu (2018). “Germanium Fin Tunnel Field Effect Transistor with Abrupt Tunnel Junction and Large Tunneling Area”. IEEE Trans. Electron Devices 59(2), pp. 292–301.
17. Debnath, Radhe Gobinda (2020). “Impact of source-doping gradient in terms of lateral straggle on the performance of germanium epitaxial layer double-gate TFE”. Applied Physics A 88(2), pp. 906–912.
18. Lee, Jang Woo & Young Choi (2017) “Triple-gate Tunnel FETs Encapsulated with an Epitaxial Layer for High Current Drivability” Journal of semiconductor technology and science, 17(2),pp.271-276.
19. Saha, Priyanka. “Saheli Sarkhel & Subir Kumar Sarkar “3D Modelling and Performance Analysis of Dual Material Tri-Gate Tunnel Field Effect Transistor”. IETE Technical Review.
20. Ghazaly, N. M. . (2022). Data Catalogue Approaches, Implementation and Adoption: A Study of Purpose of Data Catalogue. International Journal on Future Revolution in Computer Science &Amp; Communication Engineering, 8(1), 01–04. https://doi.org/10.17762/ijfrcsce.v8i1.2063
21. Jang Hyun Kim(2019) , “Demonstration of Fin-Tunnel Field-Effect Transistor with Elevated Drain” Micromachines10(30),pp.354-362;
22. Kao, K H (2012). “Optimization of gate-on-source-only tunnel FETs with counter-doped pockets”. IEEE Trans. Electron Devices 59(8), pp. 2070–2077.
23. Kumar, M J and S Janardhanan (2013). “Doping-less tunnel field effect transistor: Design and investigation”. IEEE Transactions on Electron Devices 60(10), pp. 3285–3290.
24. Kim, Garam (2019). ‘High On-Current Ge-Channel Hetero junction Tunnel Field-Effect Transistor Using Direct Band-to-Band Tunneling, Micro machines, 77(10), pp.1-8.
25. Marjani, S, S E Hosseini, and R Faez (2016). “A 3D analytical modeling of tri-gate tunneling field-effect transistors”. Journal of Computational Electronics. Springer US 15(3), pp. 820–830.
26. Najam, Faraz (2019). “Impact of Quantum Confinement on Band-to-Band Tunneling of Line-Tunneling Type L-Shaped Tunnel Field-Effect Transistor”. IEEE Transactions on Electron Devices 66(4), pp. 2010–2016.
27. A.K Dharmireddy, ,A.Sharma, M.Sushanth Babu, Sreenivasa Rao Ijjada (2020) “SS < 30 mV/dec; Hybrid tunnel FET 3D analytical model for IoT applications” Materials Today: Proceedings Elsevier publications, https://doi.org/10.1016 /j.matpr.2020.09.367 .
28. Dash, D. K. et al. (2019) ‘3D analytical modeling and electrical characteristics analysis of gate engineered SiO2/HfO2-stacked tri-gate TFET’ Indian journal of physics, 94(2), pp.219-232.
29. A. Chawla, “Phishing website analysis and detection using Machine Learning”, Int J Intell Syst Appl Eng, vol. 10, no. 1, pp. 10–16, Mar. 2022.
30. Villacorta, H, J Segura, and V Champac (2016). “Impact of Fin-Height on SRAM Soft Error Sensitivity and Cell Stability”. Journal of Electronic Testing, pp. 307–314
31. Gupta, D, N Bagga, and S Das gupta (2018). “Reduced Gate Capacitance of Dual Metal Double Gate over Single Metal Double Gate Tunnel FET: A Comparative Study”. Proc. IEEE Conference on Emerging Devices and Smart Systems, pp. 110–112.

32. Rosca, T (2018). "An Experimental Study of Hetero structure Tunnel FET Nanowire Arrays: Digital and Analog Figures of Merit from 300K to 10K". Technical Digest - International Electron Devices Meeting, IEDM. IEEE.
33. Noor, S L, S Safa, and M Z R Khan (2017). "A silicon-based dual-material double-gate tunnel field-effect transistor with optimized performance". International Journal of Numerical Modelling: Electronic Networks, Devices and Fields (6), pp. 30–30.
34. A. B. YILMAZ, Y. S. TASPINAR, and M. Koklu, "Classification of Malicious Android Applications Using Naive Bayes and Support Vector Machine Algorithms", Int J Intell Syst Appl Eng, vol. 10, no. 2, pp. 269–274, May 2022.
35. S.Kumar (2017), '2-D Analytical Modeling of the Electrical Characteristics of Dual-Material Double Gate TFETs with a SiO2/HfO2 Stacked Gate-Oxide Structure', IEEE Transactions on Electron Devices, 64(3), pp. 960-968.
36. Xu, P (2017). "Compact Model for Double-Gate Tunnel FETs with Gate-Drain Underlap". IEEE Transactions on Electron Devices 64(12), pp. 5242–5246.

Appendix A.

$$\alpha = \frac{2\left(1+\frac{C_f}{C_b}+\frac{C_f}{C_{si}}\right)}{t_{si}^2\left(1+2\frac{C_{si}}{C_b}\right)};$$

$$\beta_1 = \frac{qN_A}{\varepsilon_{si}} - 2V'_{GS1}\left(\frac{2\left(1+\frac{C_f}{C_b}+\frac{C_f}{C_{si}}\right)}{t_{si}^2\left(1+2\frac{C_{si}}{C_b}\right)}\right) - 2V'_{sub}\left(\frac{1}{t_{si}^2\left(1+2\frac{C_{si}}{C_b}\right)}\right);$$

$$\beta_2 = \frac{qN_A}{\varepsilon_{si}} - 2V'_{GS2}\left(\frac{2\left(1+\frac{C_f}{C_b}+\frac{C_f}{C_{si}}\right)}{t_{si}^2\left(1+2\frac{C_{si}}{C_b}\right)}\right) - 2V'_{sub}\left(\frac{1}{t_{si}^2\left(1+2\frac{C_{si}}{C_b}\right)}\right);$$

$$\lambda_1 = \sqrt{\alpha} = \sqrt{\frac{2\left(1+\frac{C_f}{C_b}+\frac{C_f}{C_{si}}\right)}{t_{si}^2\left(1+2\frac{C_{si}}{C_b}\right)}}; \qquad \lambda_2 = -\sqrt{\alpha} = -\sqrt{\frac{2\left(1+\frac{C_f}{C_b}+\frac{C_f}{C_{si}}\right)}{t_{si}^2\left(1+2\frac{C_{si}}{C_b}\right)}};$$

From 32(a) and 32(b) the constants of A, B, C and D values are

$$A = \left\{\frac{(V_{bi}-\sigma_2+V_{ds}) - \exp\left(-\lambda_1(L_1-L_2)(V_{bi}-\sigma_1)\right) - (\sigma_1-\sigma_2)\cos(\lambda_1 L_2)}{1-\exp\left(-2\lambda_1(L_1+L_2)\right)}\right\}\exp\left(-\lambda_1(L_1+L_2)\right)$$

$$B = \left\{\frac{(V_{bi}-\sigma_1) - (V_{bi}-\sigma_2+V_{ds}) - \exp\left(-\lambda_1(L_1+L_2)\right) - (\sigma_1-\sigma_2)\cos(\lambda_1 L_2)}{1-\exp\left(-2\lambda_1(L_1+L_2)\right)}\right\}\exp\left(-\lambda_1(L_1+L_2)\right)$$

$$C = A\exp(\lambda_1 L_1) + \frac{(\sigma_1-\sigma_2)}{2};$$

$$D = B\exp(\lambda_2 L_1) + \frac{(\sigma_1-\sigma_2)}{2};$$

$$\alpha_{asym} = \frac{2\left(1+\frac{C_{OX}}{C_{OXb}}+\frac{C_{OX}}{C_{Si}}\right)}{\left(\left(H_{fin}^2\left[\left(1+\frac{2C_{si}}{C_{oxb}}\right)\left(1+\frac{\varepsilon_{si}}{C_{ox}}\right)\right]\right)-\left(1+\frac{C_{OX}}{C_{OXb}}+\frac{C_{OX}}{C_{Si}}\right)Y^2\right)}$$

$$\beta_{asym1} = \frac{\left(\left(\frac{qN_a}{\epsilon_{si}}\right)\left(\left(H_{fin}^2\left[\left(1+\frac{2C_{si}}{C_{oxb}}\right)\left(1+\frac{\varepsilon_{si}}{C_{ox}}\right)\right]\right)-\left(1+\frac{C_{OX}}{C_{OXb}}+\frac{C_{OX}}{C_{Si}}\right)Y^2\right)-2\left(\left(\frac{C_{OX}}{C_{OXb}}+\frac{C_{OX}}{C_{Si}}\right)V'_{GS1}+V'_{SUB}+\left(\frac{C_{OX}}{\varepsilon_{Si}}\right)Y(V'_{SUB}-V'_{GS1})\right)\right)}{\left(\left(H_{fin}^2\left[\left(1+\frac{2C_{si}}{C_{oxb}}\right)\left(1+\frac{\varepsilon_{si}}{C_{ox}}\right)\right]\right)-\left(1+\frac{C_{OX}}{C_{OXb}}+\frac{C_{OX}}{C_{Si}}\right)Y^2\right)}$$

$$\beta_{asym2}=\frac{\left(\left(\frac{qN_a}{\epsilon_{si}}\right)\left(\left(H_{fin}^2\left[\left(1+\frac{2C_{si}}{C_{oxb}}\right)\left(1+\frac{\varepsilon_{si}}{C_{ox}}\right)\right]\right)-\left(1+\frac{C_{OX}}{C_{OXb}}+\frac{C_{OX}}{C_{Si}}\right)Y^2\right)-2\left(\left(\frac{C_{OX}}{C_{OXb}}+\frac{C_{OX}}{C_{Si}}\right)V'_{GS2}+V'_{SUB}+\left(\frac{C_{OX}}{\varepsilon_{Si}}\right)Y(V'_{SUB}-V'_{GS1})\right)\right)}{\left(\left(H_{fin}^2\left[\left(1+\frac{2C_{si}}{C_{oxb}}\right)\left(1+\frac{\varepsilon_{si}}{C_{ox}}\right)\right]\right)-\left(1+\frac{C_{OX}}{C_{OXb}}+\frac{C_{OX}}{C_{Si}}\right)Y^2\right)}$$

$$A_1 = \frac{\left[(V_{bi}-\sigma_{asym2}+V_{DS})-\left(\exp(-\lambda_{1a}(L_1+L_2)(V_{bi}-\sigma_{asym1})-\left((\sigma_{asym1}-\sigma_{asym2})(\cosh(\lambda_{1a}L_2))\right)\right)\right](\exp(-\lambda_{1a}(L_1+L_2))}{1-\exp(-2\lambda_{1a}(L_1+L_2))}$$

$$B_1 = \frac{\left[(V_{bi}-\sigma_{asym1})-(V_{bi}-\sigma_{asym2}+V_{DS})(\exp(-\lambda_{1a}(L_1+L_2))-\left((\sigma_{asym1}-\sigma_{asym2})(\exp(-\lambda_{1a}(L_1+L_2))(\cosh(\lambda_{1a}L_2))\right)\right]}{1-\exp(-2\lambda_{1a}(L_1+L_2))}$$

$$C_1 = \frac{A_1(\exp(\lambda 1a\ L1))-(\sigma asym1-\sigma asym2)}{2};$$

$$D_1 = \frac{B_1(\exp(\lambda 2a\ L1))-(\sigma asym1\ -\ \sigma asym2)}{2}$$

Appendix B.

$$\lambda_{sym}=\sqrt{\frac{\varepsilon_{si}t_{ox}W_{fin}}{4\varepsilon_{ox}}\left(1+\frac{\varepsilon_{ox}}{\varepsilon_{si}}\frac{W_{fin}}{4t_{ox}}\right)}\ ;\ \lambda_{asym}=\frac{1}{2}\sqrt{\frac{\varepsilon_{si}t_{oxb}H_{fin}(2\varepsilon_{si}t_{ox}+H_{fin})}{\varepsilon_{ox}[\varepsilon_{si}(t_{ox}+t_{oxb})+\varepsilon_{ox}H_{fin}]}};$$

$$A(\lambda)=\frac{e^{\frac{4L}{\lambda}}-2e^{\frac{2L}{\lambda}}+1}{\left(e^{\frac{L}{\lambda}}-1\right)^4};\qquad B(\lambda)=\frac{2e^{\frac{3L}{\lambda}}-4e^{\frac{2L}{\lambda}}+2e^{\frac{L}{\lambda}}}{\left(e^{\frac{L}{\lambda}}-1\right)^4};\qquad C(\lambda)=\frac{2e^{\frac{L}{2\lambda}}\left(1+e^{\frac{L}{\lambda}}\right)}{\left(e^{\frac{L}{\lambda}}-1\right)^2};$$

$$K_1=\frac{\varepsilon_{si}t_{oxb}}{\varepsilon_{si}(t_{ox}+t_{oxb})+\varepsilon_{ox}H_{fin}};\qquad K_2=\frac{[q(\varepsilon_{si}/\varepsilon_{ox})N_at_{ox}t_{oxb}H_{fin}]+[\varepsilon_{si}\varphi_{ms}(t_{ox}+t_{oxb})-\varepsilon_{ox}(H_{fin}V_{gsb}-\varphi_{ms}H_{fin})]\left[\varepsilon_{si}t_{ox}V_{gsb}-\frac{1}{2}qN_aH_{fin}^2t_{oxb}\right]}{\varepsilon_{si}(t_{ox}+t_{oxb})+\varepsilon_{ox}H_{fin}}$$

$$A(\lambda_{asym})=\frac{e^{\frac{4L}{\lambda}}-2e^{\frac{2L}{\lambda}}+1}{\left(e^{\frac{L}{\lambda}}-1\right)^4}\left(\frac{1}{2}\sqrt{\frac{\varepsilon_{si}t_{oxb}H_{fin}(2\varepsilon_{si}t_{ox}+H_{fin})}{\varepsilon_{ox}[\varepsilon_{si}(t_{ox}+t_{oxb})+\varepsilon_{ox}H_{fin}]}}\right);$$

$$B(\lambda_{asym})=\frac{2e^{\frac{3L}{\lambda}}-4e^{\frac{2L}{\lambda}}+2e^{\frac{L}{\lambda}}}{\left(e^{\frac{L}{\lambda}}-1\right)^4}\left(\frac{1}{2}\sqrt{\frac{\varepsilon_{si}t_{oxb}H_{fin}(2\varepsilon_{si}t_{ox}+H_{fin})}{\varepsilon_{ox}[\varepsilon_{si}(t_{ox}+t_{oxb})+\varepsilon_{ox}H_{fin}]}}\right);$$

$$C(\lambda_{asym})=\frac{2e^{\frac{L}{2\lambda}}\left(1+e^{\frac{L}{\lambda}}\right)}{\left(e^{\frac{L}{\lambda}}-1\right)^2}\left(\frac{1}{2}\sqrt{\frac{\varepsilon_{si}t_{oxb}H_{fin}(2\varepsilon_{si}t_{ox}+H_{fin})}{\varepsilon_{ox}[\varepsilon_{si}(t_{ox}+t_{oxb})+\varepsilon_{ox}H_{fin}]}}\right);$$

Appendix C.

$$G_1=A(\lambda_{sym})=\frac{e^{\frac{4L}{\lambda}}-2e^{\frac{2L}{\lambda}}+1}{\left(e^{\frac{L}{\lambda}}-1\right)^4}\left(\sqrt{\frac{\varepsilon_{si}t_{ox}W_{fin}}{4\varepsilon_{ox}}\left(1+\frac{\varepsilon_{ox}}{\varepsilon_{si}}\frac{W_{fin}}{4t_{ox}}\right)}\right);$$

$$G_2=B(\lambda_{sym})=\frac{2e^{\frac{3L}{\lambda}}-4e^{\frac{2L}{\lambda}}+2e^{\frac{L}{\lambda}}}{\left(e^{\frac{L}{\lambda}}-1\right)^4}\left(\sqrt{\frac{\varepsilon_{si}t_{ox}W_{fin}}{4\varepsilon_{ox}}\left(1+\frac{\varepsilon_{ox}}{\varepsilon_{si}}\frac{W_{fin}}{4t_{ox}}\right)}\right);$$

$$G_3=C(\lambda_{sym})=\frac{2e^{\frac{L}{2\lambda}}\left(1+e^{\frac{L}{\lambda}}\right)}{\left(e^{\frac{L}{\lambda}}-1\right)^2}\left(\sqrt{\frac{\varepsilon_{si}t_{ox}W_{fin}}{4\varepsilon_{ox}}\left(1+\frac{\varepsilon_{ox}}{\varepsilon_{si}}\frac{W_{fin}}{4t_{ox}}\right)}\right);$$

$$H_1 = \frac{A(\lambda_{asym})}{K_1} = \left[\left(\frac{e^{\frac{4L}{\lambda}} - 2e^{\frac{2L}{\lambda}} + 1}{\left(e^{\frac{L}{\lambda}} - 1\right)^4}\right)\left(\frac{1}{2}\sqrt{\frac{\varepsilon_{si} t_{oxb} H_{fin}(2\varepsilon_{si} t_{ox} + H_{fin})}{\varepsilon_{ox}[\varepsilon_{si}(t_{ox} + t_{oxb}) + \varepsilon_{ox} H_{fin}]}}\right)\left(\frac{\varepsilon_{si}(t_{ox} + t_{oxb}) + \varepsilon_{ox} H_{fin}}{\varepsilon_{si} t_{oxb}}\right)\right];$$

$$H_2 = \frac{B(\lambda_{asym})}{K_1} = \left[\left(\frac{2e^{\frac{3L}{\lambda}} - 4e^{\frac{2L}{\lambda}} + 2e^{\frac{L}{\lambda}}}{\left(e^{\frac{L}{\lambda}} - 1\right)^4}\right)\left(\frac{1}{2}\sqrt{\frac{\varepsilon_{si} t_{oxb} H_{fin}(2\varepsilon_{si} t_{ox} + H_{fin})}{\varepsilon_{ox}[\varepsilon_{si}(t_{ox} + t_{oxb}) + \varepsilon_{ox} H_{fin}]}}\right)\left(\frac{\varepsilon_{si}(t_{ox} + t_{oxb}) + \varepsilon_{ox} H_{fin}}{\varepsilon_{si} t_{oxb}}\right)\right];$$

$$H_3 = \frac{C(\lambda_{asym})}{K_1} = \left[\left(\frac{2e^{\frac{L}{2\lambda}}\left(1 + e^{\frac{L}{\lambda}}\right)}{\left(e^{\frac{L}{\lambda}} - 1\right)^2}\right)\left(\frac{1}{2}\sqrt{\frac{\varepsilon_{si} t_{oxb} H_{fin}(2\varepsilon_{si} t_{ox} + H_{fin})}{\varepsilon_{ox}[\varepsilon_{si}(t_{ox} + t_{oxb}) + \varepsilon_{ox} H_{fin}]}}\right)\left(\frac{\varepsilon_{si}(t_{ox} + t_{oxb}) + \varepsilon_{ox} H_{fin}}{\varepsilon_{si} t_{oxb}}\right)\right];$$